Model for the magnetomechanical behavior of NiMnGa driven with collinear field and stress

Xiang Wang and Marcelo J. Dapino

Department of Mechanical Engineering, The Ohio State University, Columbus, OH 43202, USA

ABSTRACT

This paper presents a model for NiMnGa transducers driven with collinear magnetic fields and stresses. Prior work by the authors demonstrates the existence of reversible strains under the application of collinear magnetic fields and stresses oriented along the [001] crystallographic axis of a cylindrical rod of single-crystal $Ni_{50}Mn_{28.7}Ga_{21.3}$. Internal bias stresses from pinning sites in the material are believed to provide the restoring force which allows for the reversibility of the strain. A constitutive model to describe the motion of twin boundaries in the presence of energetically strong pinning sites is presented. The effective pinning strength is represented by an internal bias stress oriented transversely. Stochastic homogenization is then used to account for variability in the bias stresses throughout the material and inhomogeneity in the interaction field intensity. The internal rod dynamics are modeled through force balancing with boundary conditions dictated by the constructive details of the transducer and mechanical load. The model is formulated in variational form, resulting in a second-order temporal system with magnetic field induced strain as the driving mechanism. Model result for unloaded conditions is compared with experimental measurements.

Keywords: Ferromagnetic shape memory alloys, Ni-Mn-Ga, magnetic transducers

1. INTRODUCTION

Much attention has been given to the development and understanding of ferromagnetic shape memory alloys (FSMAs) in the nickel manganese gallium (NiMnGa) system. Large bidirectional strains of up to 10% are produced in these alloys by twin boundary motion as martensite variants rotate to align respectively parallel or perpendicular to applied magnetic fields or stresses. Compared with other smart materials, for example piezoceramics and magnetostrictive materials, NiMnGa can potentially achieve both high bandwidth and large strains in response to magnetic fields. Piezoceramic and magnetostrictive materials have high response frequencies, but they can produce only small strains on the order of 10^{-3}. Shape memory alloys can produce very large strains in excess of 8% in tension, but at the expense of slow response due to the restriction of thermal conduction.

In the Heusler alloy Ni_2MnGa, cooling below the characteristic martensite start temperature M_s produces a cubic to tetragonal transformation and a corresponding twin-variant structure. Over a certain compositional range, a typical martensite microstructure consists of a mixture of three variants, each with tetragonal lattice c×c×a (c/a=0.94), in which adjacent variants are separated by a boundary known as a twin plane. Large magnetic field-induced strain (MFIS) results from the reorientation of favorable martensite variants through the motion of twin boundaries. Either magnetic fields or stresses can be used to transform the material to a single variant. Since both magnetic fields and compressive stresses favor alignment of the short c-axis of the tetragonal unit cell, in actuator applications a fixed stress oriented perpendicular to the drive field is usually applied to restore the twin variants and obtain reversible MFIS when the drive field is cycled. This is implemented by placing a rectangular alloy in an electromagnet with the drive field applied along the [110] direction and the load axis oriented along the [001] direction - both directions relative to the parent austenite phase.

We have established[1] that large reversible strains of −0.41% are possible in single crystal $Ni_{50}Mn_{28.7}Ga_{21.3}$ exposed to alternating magnetic fields along the [001] direction of the parent austenite phase and no external restoring force. This result is significant because it enables a new class of solenoid-based NiMnGa transducers like

---

Further author information: (Send correspondence to M.J.D.)
X.W.: E-mail: wang.905@osu.com, Telephone: 1-614-247-7480
M.J.D.: E-mail: dapino.1@osu.edu, Telephone: 1-614-688-3689

that shown in Fig. 1b. This transducer architecture includes a path for flux return and is thus significantly more compact, lightweight and energy efficient than conventional electromagnet devices (Fig. 1a). It is emphasized that the underlying behavior cannot be explained by existing models for martensitic variant reorientation based on the competing effects of the stress energy and Zeeman energy as the latter attempts to overcome the twin boundary energy. This points to the existence of bias or residual stresses built in the alloy during the crystal growth. The bias stresses are attributed to high-strength pinning sites or point defects in the alloy which act as localized energy potentials that oppose twin boundary motion and provide an otherwise nonexisting restoring force when the magnetic field is removed. The presence of pinning sites also explains the reduced deformations relative to alloys capable of over 6% strain, in which twin boundary is largely unimpeded. Further experimental details can be found in Malla et al.[1]

The effective design and control of solenoid-based NiMnGa transducers requires understanding of the mechanisms that govern field-induced strains and quantification of the relationship between applied fields, strains and stresses in the transducer. A previous thermodynamic constitutive model[1–3] for NiMnGa driven by a collinear field and stress without external restoring forces characterizes the MFIS in the presence of pinning sites. The model employs a Gibbs energy function and corresponding energy minimization procedure to quantify twin boundary motion in the presence of an orthogonal pair formed by a uniaxial magnetic field and internal bias stresses associated with pinning sites. The model is formulated by considering the Zeeman, elastic and pinning energies. This approach constitutes an extension of work by Kiefer and Lagoudas[4] and Hirsinger and Lexcellent.[5] Although the constitutive model quantifies the local average strain for single crystal materials, it does not account for the variability in the density and strength of the pinning sites throughout the material. This variability is addressed in this paper by considering stochastic homogenization techniques that are constructed on the assumption that local Weiss-type interaction fields and pinning energies are manifestations of underlying distributions. This approach has been developed by Smith et al.[6–9] for ferroelectric materials, ferromagnetic materials and shape memory alloys.

In this paper, the constitutive model is modified to include an additional stress field associated with internal bias stresses oriented radially in a cylindrical NiMnGa sample. While the resulting formulation characterizes the MFIS, it does not account for the material dynamics as a NiMnGa driver element vibrates and does work against an external mechanical load. As a first step to that end, a dynamic transducer model is formulated by considering a NiMnGa sample connected to a spring mass damper. Force balancing yields a PDE system which is expressed in weak or variational form and subsequently solved through a Galerkin discretization in space followed by a finite-dimensional approximation of the resulting second-order temporal system. Input to the system is the force produced by MFIS, and output is the deflection at the end of the NiMnGa sample. The validity of the resulting transducer model is illustrated through comparison with experimental data.
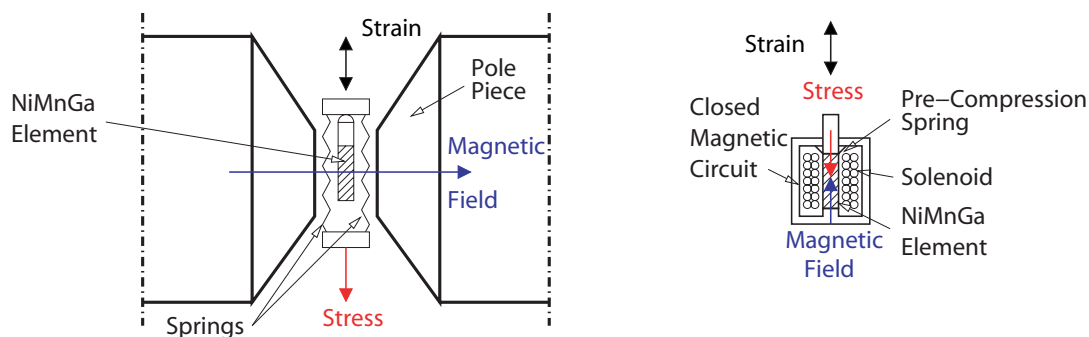

Figure 1. (a) Conventional electromagnet apparatus. (b) Solenoid transducer design and corresponding collinear field-stress drive configuration.

2. THEORY

2.1. Strain mechanism

The pinning sites that enable bidirectional MFIS without the need for external restoring forces in the marten-site are assumed in this paper to manifest as residual stresses oriented in the radial direction of a cylindrical $Ni_{50}Mn_{28.7}Ga_{21.3}$ sample. A recent study[10] has shown that Ni-Mn-Ga alloys are extremely susceptible to impurities; sulfide and tantalum inclusions, and titanium-rich precipitates have been observed. It was assumed that for the large, incoherent S and Ta inclusions observed, dislocations would have to loop around the impurities in order for twin boundary motion to occur. Since the observed Ti precipitates are much smaller than the S and Ta inclusions, it was argued that the mechanism of dislocation motion in the presence of Ti precipitates is most likely cutting through the particles, as opposed to looping. By cutting, the dislocations form two new interfaces which provide a low-energy path for dislocation movement as compared to looping around the particles. It was estimated that the small Ti-rich precipitates have a strength of approximately 0.53 K_u, thus acting as pinning sites which could be overcome by the application of sufficiently large magnetic fields. These small precipitates do not seem to impact the MFIS of the alloys studied as strains of 6% were observed.

In this context, low-energy pinning sites are assumed to not contribute to the mechanism for reversible MFIS in the alloy investigated; during the first few field cycles after manufacture of the alloy, the twin boundaries have unattached from these sites and permanently attached to higher-energy sites. Hence, the twin boundaries are normally pinned to point defects whose energy is greater than the anisotropy energy (Fig. 2). When a small magnetic field is applied along the [001] direction, the twin boundaries attempt to displace according to the standard mechanisms for twin variant reorientation, but the Zeeman energy that drives the motion of the twin boundaries is insufficient to completely overcome the energy potential of the pinning sites. Instead, the twin boundaries loop around the impurities and as they do work against the pinning sites, energy is dissipated. Saturation is achieved when the Zeeman energy is large enough to overcome the anisotropy energy and the magnetic moments become aligned with the field without changing the orientation of the crystal. When the field is removed, the anisotropy energy returns the magnetic moments to the easy c-axis of the crystal and the pinning site energy provides a restoring mechanism for the twin boundaries, returning the sample to its original length and magnetization value. The pinning energy can thus be interpreted as an internal bias stress σ_x oriented perpendicular to the [001] direction, as shown in Fig. 2. Due to the competing effect of the internal bias stress and the external magnetic field, excessive pinning energy would render the alloy inactive as the available Zeeman pressure would be insufficient to drive the motion of twin boundaries away from the pinning sites. This theory provides an explanation not only for the reversibility of the strain in the absence of an externally applied stress or field, but also the smaller magnitude of strain generated from the sample investigated.

2.2. Constitutive model

To model the behavior discussed in the previous section, the pinning site energy is incorporated in this paper by assuming that pinning sites create an effective bias stress σ_x oriented along the radial direction of the rod. While
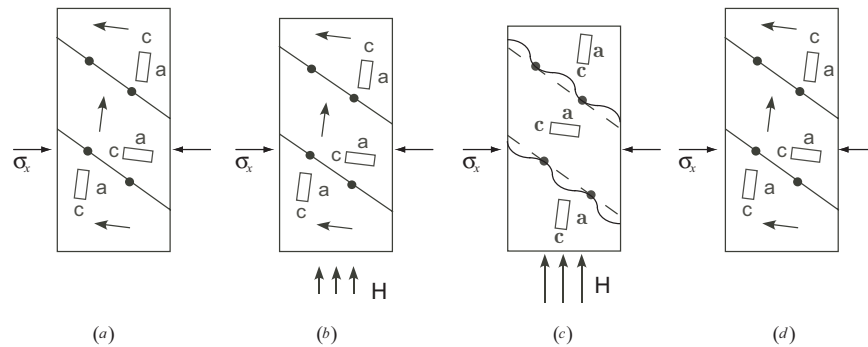

Figure 2. Strain mechanism for FSMA under collinear stress and magnetic field.

Faidley et al.[3] employed a thermodynamic framework which is similar to the one presented here, they modeled the pinning sites as springs whose potential energy follows a quadratic law on the volume fraction. This energy was shown to have a form similar to the hardening function employed by Kiefer and Lagoudas[4] on the basis of shape memory arguments. The structure is represented by the simplified two-variant system shown in Fig. 3. The energy for this system is given by

$$G(\boldsymbol{\sigma}, \mathbf{H}, T) = (1 - \xi)G^{V1} + \xi G^{V2} \tag{1}$$

where G^{Vi} is the energy of the i-th variant. Variant 1 is the transverse variant with the easy magnetization direction perpendicular to the field and a volume fraction of $(1 - \xi)$; variant 2 is that which is favored by the applied field and has a volume fraction of ξ.

In order to determine G^{Vi}, two assumptions are made: (i) the system is isothermal and (ii) the fields are large enough to ensure that the effects of the magnetic domains can be ignored. The energy of each variant can be written as

$$G^{Vi}(\boldsymbol{\sigma}, \mathbf{H}, T = const) = \psi^{Vi} - \frac{1}{2\rho}\boldsymbol{\sigma} : \mathbf{S}^{Vi}\boldsymbol{\sigma} - \frac{\mu_0}{\rho}\mathbf{M}^{Vi} \cdot \mathbf{H} \tag{2}$$

where ψ is the Helmholtz energy, $\boldsymbol{\sigma}$ is the applied stress, $\mathbf{S}$ is the mechanical compliance, $\mathbf{M}$ is the magnetization, $\mathbf{H}$ is the applied field, ρ is the density, and μ_0 is the permeability of free space. The component σ_x in $\boldsymbol{\sigma}$ matrix is considered as a linear function of volume fraction ξ, $\sigma_x = k\xi$.

Substitution of (2) into (1) gives the energy for the system:

$$G(\boldsymbol{\sigma}, \mathbf{H}, T = const) = \psi^{V1} - \frac{1}{2\rho}S_{yy}^{V_1}\sigma_y^2 - \xi\frac{\mu_0}{\rho}M_sH - \begin{cases} b_1\xi + a_1\xi^2 & \dot{\xi} > 0 \\ b_2\xi + a_2\xi^2 & \dot{\xi} < 0 \end{cases} \tag{3}$$

where $a = \frac{1}{2\rho}k^2S_{11}^{V_1}$ and $b = \frac{1}{\rho}kS_{12}^{V_1}$. The two variants are assumed to have the same compliance; $\Delta\psi = 0$ is also zero since the Helmholtz energies of the two variants are identical. The free energy expression can be used to obtain various thermodynamic quantities. In this case, the volume fraction is quantified by combining relation (3) with the Clausius-Duhem version of the second law of thermodynamics[4]

$$\pi^\xi = \epsilon_s\sigma_y - \rho\frac{\partial G}{\partial \xi} \tag{4}$$

where $\pi^\xi = \pm Y^\xi$ is the condition for the onset of twin variant motion and ϵ_s is the saturation strain. This yields an expression for the detwinning force

$$\pm Y^\xi = \epsilon_s\sigma_y + \mu_0M_sH_y + \rho\begin{cases} b_1 + 2a_1\xi & \dot{\xi} > 0 \\ b_2 + 2a_2\xi & \dot{\xi} < 0 \end{cases}. \tag{5}$$
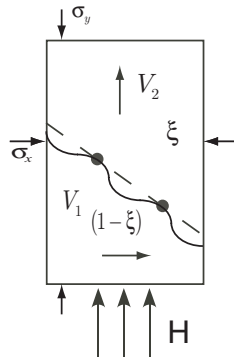

Figure 3. Two-dimensional variants: notation and orientation.

Equation (5) can be solved for the volume fraction

$$\xi = \begin{cases} \frac{1}{2\rho a_1}(-\epsilon_s \sigma_y - \mu_0 M_s H_y + \rho b_1 + Y^\xi) & \dot{\xi} > 0 \\ \frac{1}{2\rho a_2}(-\epsilon_s \sigma_y - \mu_0 M_s H_y + \rho b_2 - Y^\xi) & \dot{\xi} < 0 \end{cases}. \tag{6}$$

2.3. Stochastic homogenization

Equation (6) provides a model for the strain generated by single crystal NiMnGa when exposed to collinear magnetic fields and external stresses. The accuracy of this model is limited due to the following factors: (i) The sample is assumed to consist of only two variants with a single boundary. In reality, however, Ni-Mn-Ga has many twin variants though only two distinct orientations. This implies that a sample will have numerous twin boundaries and thus numerous pinning sites. (ii) The pinning sites and effective bias stress are assumed to be homogeneously distributed throughout the material and every pinning site is assumed to have the same energy. As discussed by Marioni,[11] in a physical material the pinning energies vary over a large range which translates into a variation of σ_x. (iii) The magnetic field is assumed to be uniform throughout the sample. However, due to short-range interactions the magnetic field in Ni-Mn-Ga can be considered to behave locally in a fashion similar to the Weiss mean field.[12] Thus, the magnitude of the field at a given point in the material is not equal to the applied field but rather, is given by an effective field which is dependent on the applied field and the magnetization, $H_e = H + H_i = H + \alpha M$. The mean field constant α varies from point to point in the material due to differences in the lattice structure.

The above limitations are addressed by considering stochastic homogenization as proposed by Smith.[7] This approach has been proven effective in the modeling of hysteresis and constitutive nonlinearities in ferroelectric compounds, ferromagnetic materials, and shape memory alloys. For implementation, the bias stress and the interaction field are treated as statistical distributions, which results in a macroscopic model for the volume fraction of the form

$$[\xi(H, \sigma)](t) = \int_0^\infty \int_{-\infty}^\infty \nu_1(H_i)\nu_2(a_2) \left[\bar{\xi}(H + H_i, \sigma, a_2)\right](t)dH_i da_2 \tag{7}$$

where ν_1 and ν_2 respectively denote the probability distribution functions for (H_i) and (a_2), and $\bar{\xi}$ is given by (6). Since the interaction field can be both positive and negative, a normal distribution centered at will be an appropriate choice

$$\nu_1(H_i) = c_1 e^{-H_i^2/(2b^2)} \tag{8}$$

Since a_2 has to be non-negative, a lognormal distribution is considered

$$\nu_2(a_2) = c_2 e^{-(\ln(a_2/\overline{a_2})/2c)^2}. \tag{9}$$

The strain is related to the volume fraction by

$$\epsilon = \xi \epsilon_{th}, \tag{10}$$

with ϵ_{th} the maximum theoretical strain which would occur if a single boundary swept through the entire material, thus producing a change in ξ from 0 to 1. Hence, for the case where the twin boundaries are restrained by pinning sites, ξ will be limited to a much smaller range.

3. TRANSDUCER MODEL

3.1. Variational form

A one-dimensional representation of the transducer is shown in Fig. 4. The NiMnGa rod is assumed to be homogeneous with length l, cross-section area A and longitudinal coordinate x. The density, Young's modulus and Kelvin-Voigt damping coefficient are respectively denoted by ρ, E and c. The end at $x = 0$ is considered fixed and the other end is connected to a mass m_l, a spring with stiffness k_l and a damper with coefficient c_l.
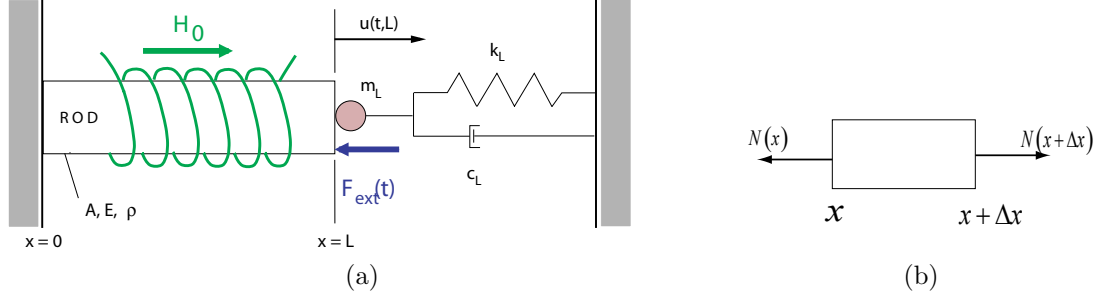
Figure 4. (a) Representation of a NiMnGa transducer; (b) infinitesimal element considered for force analysis.

To quantify the dynamics of the rod, we consider an infinitesimal element $[x, x + \Delta x]$ as depicted in Fig. 4(b). The stress at a point $\sigma(x, t)$ is given by:

$$\sigma(t, x) = E\frac{\partial u}{\partial x}(t, x) + c\frac{\partial^2 u}{\partial x \partial t}(t, x) - E\epsilon(t, x) \tag{11}$$

where ϵ is the MFIS described by relation (6). When integrated across the rod, this yields the inplane resultant

$$N(t, x) = \int_A \sigma \, dA = \sigma(t, x)A = EA\frac{\partial u}{\partial x}(t, x) + cA\frac{\partial^2 u}{\partial x \partial t}(t, x) - EA\epsilon(t, x). \tag{12}$$

The balance of forces for the element can be expressed as

$$N(t, x + \Delta x) - N(t, x) = \int_x^{x+\Delta x} \rho A \frac{\partial^2 u}{\partial t^2}(t, x) \, dx \tag{13}$$

which yields

$$\frac{\partial N}{\partial x}(t, x) = \rho A \frac{\partial^2 u}{\partial^2 t}(t, x) \tag{14}$$

as a strong form of the model for the internal rod dynamics.

To obtain appropriate boundary conditions, it is first noted that the end at $x = 0$ satisfies the condition $u(t, 0) = 0$. At the end $x = L$, force balance yields the second boundary condition

$$N(t, L) = -k_l u(t, L) - c_l \frac{\partial u}{\partial x}(t, L) - m_l \frac{\partial^2 u}{\partial x^2}(t, L).$$

Thus the boundary conditions can be summarized as

$$\begin{cases} u(t, 0) = 0 \\ N(t, L) = -k_l u(t, L) - c_l \frac{\partial u}{\partial x}(t, L) - m_l \frac{\partial^2 u}{\partial x^2}(t, L) \end{cases} . \tag{15}$$

The initial conditions are

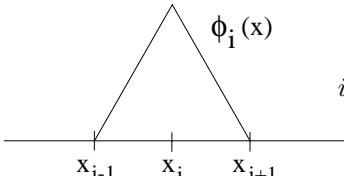$$\begin{cases} u(0, x) = 0 \\ \frac{\partial u}{\partial x}(0, x) = 0 \end{cases} . \tag{16}$$

The combination of (14)-(16) yields the strong form of the model. To find a solution to this system of equations, we consider the weak form of the model, which is developed either via integration by parts or Hamiltonian energy principles. In weak form, displacements and tests functions are differentiated only once compared with the second derivatives required in the strong form. This reduces the smoothness requirements on the finite element basis when constructing an approximation method.

To construct a weak form of the model, we consider the state u in the state space $X = L^2(0, L)$, and the space of test functions is taken to be $V = H^1_L(0, L) \equiv \{\phi \in H^1(0, L) \mid \phi(0) = 0\}$.[13] Multiplication by test functions followed by integration over the length of the rod yields the weak form of the model. For all $\phi \in V$
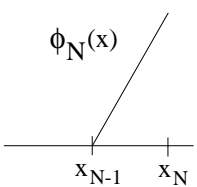
$$\int_0^L \rho A \frac{\partial^2 u}{\partial t^2} \phi \, dx = - \int_0^L \left[EA \frac{\partial u}{\partial x}(t,x) + cA \frac{\partial^2 u}{\partial x \partial t} - EA\epsilon(t,x) \right] \frac{\partial \phi}{\partial x} \, dx - \left[k_l u(t,L) + c_l \frac{\partial u}{\partial t}(t,L) + m_l \frac{\partial^2 u}{\partial t^2} \right]. \quad (17)$$

3.2. Numerical approximation

To approximate a solution to relation (17), we consider a Galerkin discretization followed by a finite difference approximation of the resulting temporal system. To this end, the interval $[0, L]$ is partitioned in N subintervals of stepsize $h = L/N$. The spatial basis is comprised of linear splines or "hat functions",[14] defined at points $x_i = i\, h$ $(i = 0, 1, \ldots, N)$ as follows

$$\phi_i(x) = \frac{1}{h} \begin{cases} (x - x_{i-1}), & x_{i-1} \le x < x_i \\ (x_{i+1} - x), & x_i \le x < x_{i+1} \\ 0, \text{ otherwise} \end{cases} \qquad i = 1, \ldots, N-1$$

$$\phi_i(x) = \frac{1}{h} \begin{cases} (x - x_{N-1}), & x_{N-1} \le x \le x_N \\ 0, \text{ otherwise.} \end{cases}$$

The displacements $u(t,x)$ are approximated using the expansion

$$u^N(t,x) = \sum_{j=1}^{N} u_j(t) \phi_j(x), \quad (18)$$

defined in the subspace $H^N = \text{span}\{\phi_j\}_{j=1}^N$, which through the construction of the basis functions satisfies the respective boundary conditions in the transducer.

The approximate solution (18) is substituted into (17), along with test functions ϕ equal to the basis functions, to form a second-order temporal vector system

$$M \ddot{\vec{u}}(t) + C \dot{\vec{u}}(t) + K \vec{u}(t) = \vec{F}[\epsilon(t)], \quad (19)$$

where $\vec{u}(t) = [u_1(t), \ldots, u_N(t)]^T$.

The mass, damping and stiffness matrices have the form

$$[M]_{ij} = \begin{cases} \displaystyle\int_0^L \rho\, A\, \phi_i\, \phi_j \, dx & , \quad i \ne n \ \text{ and } \ j \ne n \\ \displaystyle\int_0^L \rho\, A\, \phi_i\, \phi_j \, dx + m_L & , \quad i = n \ \text{ and } \ j = n \end{cases}$$

$$[C]_{ij} = \begin{cases} \displaystyle\int_0^L c_D\, A\, \phi_i'\, \phi_j' \, dx & , \quad i \ne n \ \text{ and } \ j \ne n \\ \displaystyle\int_0^L c_D\, A\, \phi_i'\, \phi_j' \, dx + m_L & , \quad i = n \ \text{ and } \ j = n \end{cases}$$

$$[K]_{ij} = \begin{cases} \displaystyle\int_0^L E\, A\, \phi_i'\, \phi_j' \, dx & , \quad i \ne n \ \text{ and } \ j \ne n \\ \displaystyle\int_0^L E\, A\, \phi_i'\, \phi_j' \, dx + m_L & , \quad i = n \ \text{ and } \ j = n \end{cases}$$

while the excitation vector is defined by

$$\vec{F}_i[\epsilon(t)] = \int_0^L E\,A\,\epsilon(t,x)\,\phi_i'(x)\,dx.$$

The second-order system (19) can be expressed as a first-order system of the form

$$\dot{\vec{y}}(t) = P\,\vec{y}(t) + \vec{B}(t)$$
$$\vec{y}(0) = \vec{y}_0, \tag{20}$$

where $\vec{y}(t) = [\vec{u}(t), \dot{\vec{u}}(t)]^T$ is the generalized solution, and

$$P = \begin{bmatrix} 0 & I \\ -M^{-1}K & -M^{-1}C \end{bmatrix}, \qquad \vec{B}(t) = \begin{bmatrix} 0 \\ -M^{-1}\vec{F}(t) \end{bmatrix}.$$

The first-order system (20) must be discretized in time for numerical implementation. To this end, we consider a standard trapezoidal discretization with step size Δt and iterations

$$\vec{y}_{j+1} = \mathcal{P}\,\vec{y}_j + \tfrac{1}{2}\,\mathcal{B}\left[\vec{B}(t_j) + \vec{B}(t_{j+1})\right]$$
$$\vec{y}_0 = \vec{y}(0),$$

where $t_j = j\Delta t$ and $\vec{y}_j$ approximates $\vec{y}(t_j)$. The matrices

$$\mathcal{P} = \left[I - \frac{\Delta t}{2}P\right]^{-1}, \qquad \mathcal{B} = \Delta t\left[I - \frac{\Delta t}{2}P\right]^{-1}$$

need only be created once when numerically or experimentally implementing the method. The accuracy of the solutions is $\mathcal{O}(h^2, (\Delta t)^2)$.

4. EXPERIMENTS AND RESULTS

To test the accuracy of the model, experiments were run on a cylindrical rod of $Ni_{50}Mn_{28.7}Ga_{21.3}$. The NiMnGa sample was actuated in a sinusoidal field of amplitude 700 kA/m and frequency 0.1 Hz. A water-cooled solenoid as described by Malla et al.[1] was employed. To minimize errors caused by the inhomogeneity of the magnetic field inside the transducer, the sample was placed in the middle of the transducer; a pick-up coil was used to monitor the magnetic flux density. The field induced strain was measured with a linear variable displacement transducer (LVDT). The system temperature was monitored with three thermocouples to ensure that the temperature of the rod was effectively controlled within $\pm 1^o F$.

For this preliminary study, only the unloaded strain vs. field behavior was chosen to test the validity of the material model. In order to determine the volume fraction in (6), parameters for the constitutive model such as $a_1, a_2, b_1, b_2, Y^\xi, M_s$ have to be identified. Among those parameters, M_s can be measured directly and Y^ξ can be obtained by the optimization process. The remaining parameters can be found by fitting to the hysteresis curve in the unloaded case, which can be found from Fig. 5 and the equations in Table 1.[1, 2]

Parameters for the external system include the loading mass m_l, which can be measured directly, external spring stiffness k_l, and damping coefficient c_l; for the NiMnGa rod, parameters to be determined are the density ρ, elastic modulus of the rod E and the Kevin-Voigt damping coefficient c. To simulate the actual experimental conditions, the spring stiffness k_l in the external system is set to zero in the model, while the damping coefficient c_l associated with the friction between the transducer push rod and bearing is obtained through fit to experimental data. The elastic modulus and the Kevin-Voigt damping coefficient are found from dynamic measurements.[15]

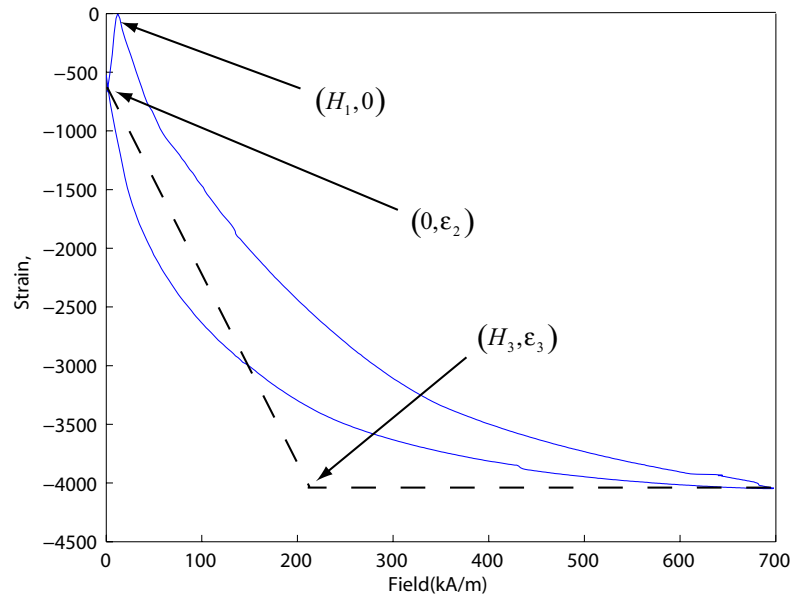Model results for the unloaded case being considered are shown in Fig 6.

Figure 5. Data points for parameters identification.

Table 1. Model parameters identified from experimental data.

$$
\begin{array}{rcl}
\epsilon & = & \xi\epsilon_{th} \\
a_1 & = & 1.5a_2 \\
a_2 & = & \frac{\mu_0 M_s H_3 \epsilon_{th}}{2(\epsilon_s - \epsilon_2)} \\
b_1 & = & \epsilon_s \sigma_y + \mu_0 M_s H_1 - Y^\xi \\
b_2 & = & \epsilon_s \sigma_y + Y^\xi - 2a_2 \frac{\epsilon_2}{\epsilon_{th}}
\end{array}
$$

5. CONCLUDING REMARKS

This paper has presented a model for NiMnGa transducers driven with collinear magnetic fields and stresses. The model is constructed in three steps. In the first, a constitutive material model for a NiMnGa rod is formulated by minimization of the Gibbs energy of a simplified, two-variant martensitic system with its boundaries pinned. The effective pinning strength is represented by an internal bias stress oriented transversely. In the second step, stochastic homogenization is used to account for variability in the bias stresses throughout the material and inhomogeneity in the interaction field intensity. For the third and last model step, a dynamic transducer model is formulated. The internal rod dynamics are modeled through force balancing with boundary conditions dictated by the constructive details of the transducer and mechanical load. Specifically, force balancing is used to construct a PDE system which is expressed in weak or variational form and subsequently solved through a Galerkin discretization in space followed by a finite-dimensional approximation of the resulting second-order temporal system. Input to the system is the force produced by MFIS, and output is the deflection at the end of the NiMnGa sample. Future work will be focused on the analytical characterization of various loading conditions.
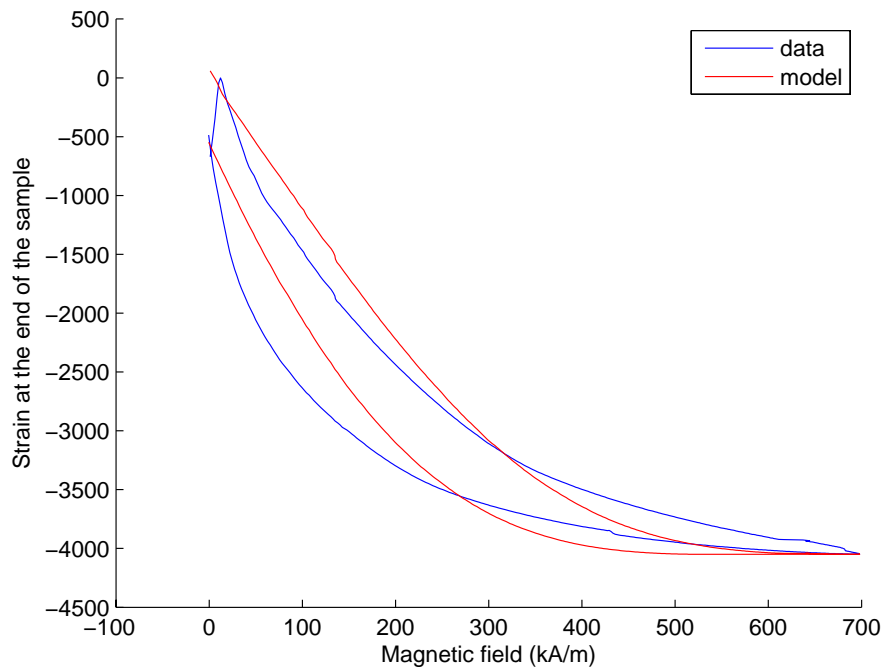
Figure 6. Comparison of model results and experimental data.

REFERENCES

1. A. Malla, M.J. Dapino, T. Lograsso and D. Schlagel, "Large magnetically-induced strains in $Ni_{50}Mn_{28.7}Ga_{21.3}$ driven with collinear field and stress." *Journal of Applied Physics,* 99(5), 1 March 2006.

2. L.E. Faidley, M.J. Dapino and G.N. Washington, "Homogenized strain model for Ni-Mn-Ga with collinear field and stress." *Journal of Intelligent Material Systems and Structures.* To appear.

3. L.E. Faidley, M.J. Dapino and G.N. Washington, "Strain model for Ni-Mn-Ga with collinear field and stress." *Proc. ASME IMECE,* Paper No. 79092, Orlando, FL, Nov. 5-11, 2005.

4. B. Kiefer and D. C. Lagoudas, "Phenomenological modeling of ferromagnetic shape memory alloys." *Proceedings of SPIE Smart Structures and Materials Conf.*, 5387, pp. 164-176, July 2004.

5. L. Hirsinger and C. Lexcellent, "Internal variable model for magneto-mechanical behaviour of ferromagnetic shape memory alloys Ni-Mn-Ga" *Journal de Physique, IV, France* 112, pp. 977-980, 2003.

6. R.C. Smith, M.J. Dapino and S. Seelecke, "A free energy model for hysteresis in magnetostrictive transducers" *Journal of Applied Physics* 93(1), pp. 458-466, 2003.

7. R. C. Smith, *Smart Material Systems: Model Development*, Society for Industrial & Applied Mathematics, Philadelphia, PA, 2005.

8. R.C. Smith and M.J. Dapino, "Stress-dependent hysteresis model for ferromagnetic transducer materials," *Proc. ASME IMECE,* Paper No. 80394, Orlando, FL, Nov. 5-11, 2005.

9. R.C. Smith, M.J. Dapino, T.R. Braun and A.P. MORTENSEN, "A homogenized energy framework for ferromagnetic hysteresis," *IEEE Transactions on Magnetics.* To appear.

10. R.L. Richard, *Systematic analysis of the crystal structure, chemical ordering, and microstructure of Ni-Mn-Ga ferromagnetic shape memory alloys,* Ph.D. Dissertation, Massachusetts Institute of Technology, Cambridge, MA, 2005.

11. M. A. Marioni, S. M. Allen, and R. C. OHandley, "Nonuniform twin-boundary motion in Ni-Mn-Ga single crystals," *Applied Physics Letters*, 84, pp. 4071-4073, May 2004.

12. D. Jiles, *Magnetism and Magnetic Materials*, Chapman & Hall, 1995.

13. M.J. Dapino, R.C. Smith and A.B. Flatau, "Structural magnetic strain model for magnetostrictive transducers," *IEEE Transactions on magnetics*, Vol 36, No. 3, May 2000.
14. P.M. Prenter, *Splines and variational methods*, New York: Wiley, 1975.
15. L. Faidley, M. Dapino, G. Washington, T. Lograsso, "Dynamic response in the low-kHz range and delta-E effect in ferromagnetic shape memory Ni-Mn-Ga.", *Proceedings of IMECE* (43198), 2003.